AJNR

Measurement of Cerebral Blood Flow in Chronic Carotid Occlusive Disease: Comparison of Dynamic Susceptibility Contrast Perfusion MR Imaging with Positron Emission Tomography

Pratik Mukherjee, Hyunseon Christine Kang, Tom O. Videen, Robert C. McKinstry, William J. Powers and Colin P. Derdeyn

AJNR Am J Neuroradiol 2003, 24 (5) 862-871
http://www.ajnr.org/content/24/5/862

Measurement of Cerebral Blood Flow in Chronic Carotid Occlusive Disease: Comparison of Dynamic Susceptibility Contrast Perfusion MR Imaging with Positron Emission Tomography

Pratik Mukherjee, Hyunseon Christine Kang, Tom O. Videen, Robert C. McKinstry, William J. Powers, and Colin P. Derdeyn

BACKGROUND AND PURPOSE: **Our purpose was to evaluate the accuracy of cerebral blood flow (CBF) measurements obtained by using dynamic susceptibility contrast-enhanced MR imaging, including the influence of arterial input function (AIF) selection, compared with those obtained by using [^{15}O]-H_2O positron emission tomography (PET) for patients with chronic carotid occlusion.**

METHODS: **MR images and PET scans were obtained of seven patients with unilateral carotid occlusion and were co-registered for region of interest analysis. PET CBF maps were generated by using the autoradiographic method. MR imaging CBF maps were calculated by deconvolution of the susceptibility time curve with a proximal middle cerebral artery AIF and were converted to absolute flow rates either by assuming a constant contralateral white matter CBF value of 22 mL/100 mL/min or by using individually determined PET white matter CBF values.**

RESULTS: **Although CBF values measured by PET and MR imaging were positively correlated for every patient, the slopes and y intercepts of the regression lines varied widely among patients. The correlation was better when individual white matter CBF values measured by PET were used to scale the white matter CBF values measured by MR imaging ($r = 0.84$, $P < .0001$) than when constant contralateral CBF values were assumed ($r = 0.54$, $P < .0001$). The choice of AIF ipsilateral or contralateral to the occluded carotid artery made no statistically significant difference ($P > .05$) to the correlation coefficient, slope, or y intercept of the MR imaging versus PET CBF regressions for six of the seven patients.**

CONCLUSION: **Although linearly correlated with CBF values measured by PET, dynamic susceptibility contrast-enhanced MR imaging was not accurate for measuring absolute CBF values. AIF selection relative to the side of carotid occlusion did not significantly affect calculated MR imaging CBF values for six of the seven patients.**

Numerous techniques exist for the noninvasive assessment of cerebral hemodynamic variables such as cerebral blood flow (CBF). These imaging modalities include positron emission tomography (PET), single photon emission CT, bolus-tracking CT, stable xenon CT, and perfusion MR imaging techniques using dynamic susceptibility contrast-enhanced MR imaging or arterial spin labeling. Dynamic susceptibility contrast-enhanced MR imaging has become a widely used technique for perfusion imaging, because MR imaging units are widely available and the examination is free of exposure to ionizing radiation or iodinated contrast agents. Dynamic susceptibility contrast-enhanced MR imaging has been used in the clinical evaluation of disorders such as stroke (1), tumors (2), and infection (3). Although dynamic susceptibility contrast-enhanced MR imaging can be used to measure CBF (4), the most popular current method for analyzing dynamic susceptibility contrast-enhanced MR imaging yields only qualitative (relative) values of CBF (5, 6). This technique relies on deconvolution

Received June 11, 2002; accepted after revision December 9.

This work was presented in part at the 39th Annual Meeting of the American Society of Neuroradiology, Boston, MA, May 2001.

Support for this work was provided by a Berlex/American Society of Neuroradiology Foundation Fellowship Award in Basic Science Research and by National Institutes of Health grants K08-NS02029 and R01–28497.

From the Mallinckrodt Institute of Radiology, Washington University School of Medicine, St. Louis, MO.

Address reprint requests to Pratik Mukherjee, MD, PhD, Diagnostic Neuroradiology, Box 0628, University of California, San Francisco, 505 Parnassus Avenue, L-358, San Francisco, CA 94143.

of the measured tissue susceptibility time curve with an arterial input function (AIF) selected from a major blood vessel near the region of interest and an estimation of relative CBF as the peak of the resulting tissue impulse response (5, 6). Additional postprocessing steps have been suggested for deriving absolute values of CBF from dynamic susceptibility contrast-enhanced MR images (7–10), and these elaborations have produced quantitative results similar to those of PET of normal humans (8), of patients with chronic cerebrovascular disease (10), and of animals in models of stroke (11). However, these quantitative MR imaging methods for measuring CBF are not yet in routine clinical use at most medical centers.

For accurate measurement of CBF by using dynamic susceptibility contrast-enhanced MR imaging, no general consensus has been reached regarding whether the AIF should be chosen ipsilateral or contralateral to the affected hemisphere in patients with unilateral carotid steno-occlusive disease (12). Theoretically, the delay in arrival time and dispersal of the IV administered bolus of contrast agent causes underestimation of CBF values (13), leading to false positive areas of acute ischemia on CBF maps of patients with carotid steno-occlusive disease if the AIF is taken from the contralateral vessel (14). Placement of an AIF distal to the stenosis or occlusion may help correct for the delay and dispersal of the bolus of contrast agent (15); however, this AIF may not accurately reflect the hemodynamics of the unaffected contralateral hemisphere. This could introduce systematic errors into CBF ratios calculated by flow normalization with the contralateral hemisphere. To our knowledge, no quantitative data regarding the influence of AIF selection on CBF measurement accuracy, as determined by comparison with an independent gold standard in patients with cerebrovascular disease, are available.

In this study of patients with chronic cerebrovascular disease, we sought to evaluate the accuracy of CBF measurement with dynamic susceptibility contrast-enhanced MR imaging, including the effects of AIF selection, by using absolute CBF measurements from [^{15}O]-H_2O PET as the gold standard. The study population consisted of patients with chronic carotid occlusion. The altered cerebral hemodynamics associated with carotid occlusion has already been extensively characterized with PET (16–18). In patients with unilateral carotid occlusion, the cerebral hemisphere contralateral to the occluded carotid artery can serve as an internal control for PET and dynamic susceptibility contrast-enhanced MR imaging measurements of CBF. Another advantage of studying chronic carotid occlusion is that it is a steady-state paradigm, unlike acute stroke, in which CBF may fluctuate rapidly because of changes in vascular resistance, development of collateral flow, or recanalization of the occluded vessel. For the purposes of this study, we used a common technique originally described by Ostergaard et al (5, 6). We compared CBF values measured by MR imaging with CBF values measured by PET in both the affected cerebral hemisphere ipsilateral to the occluded carotid artery and the control cerebral hemisphere contralateral to the occlusion. This comparison was made both for CBF values measured by MR imaging calculated with an AIF from the middle cerebral artery (MCA) ipsilateral to the occluded carotid artery and for CBF values measured by MR imaging calculated with an AIF from the MCA contralateral to the occlusion. We correlated this information with cerebral hemodynamic status, as determined from cerebral blood volume, mean transit time, and oxygen extraction fraction ratios of the affected hemisphere with the control hemisphere measured with PET.

Methods

Patients

Seven patients with unilateral occlusion of the proximal internal carotid artery were enrolled from an ongoing clinical trial of hemodynamics in chronic cerebrovascular disease. Written informed consent was obtained from every participant in accordance with the guidelines of the institutional review board at our medical center. The inclusion criterion was an angiographically confirmed atherosclerotic occlusion of one proximal internal carotid artery. Both asymptomatic and symptomatic patients were enrolled, with symptoms including transient ischemic neurologic deficits, transient monocular blindness, and mild to moderate permanent ischemic neurologic deficits in the appropriate carotid artery territory. Symptomatic patients were studied at least 1 month after their last event. Exclusion criteria were inability to provide informed consent, inability to tolerate a supine position for PET and MR imaging, pregnancy, and contraindications to MR imaging, such as claustrophobia or MR-incompatible medical implants.

Both PET and MR imaging were performed within 1 hour of each other for each patient. Just before the PET and MR imaging were performed, each patient underwent a thorough clinical evaluation by a physician investigator. Evaluation included a review of any new hospital records, CT scans, and angiograms and detailed questioning regarding any symptoms. In addition, descriptive clinical information regarding any cerebral ischemic events was collected, including occurrence and characteristics of transient ischemic attacks.

MR Imaging Protocol

All MR imaging examinations were performed on a 1.5-T system (Magnetom Vision; Siemens, Erlangen, Germany) with circularly polarized RF coils. The imaging protocol included anatomic localization with an unenhanced sagittal view 3D fast low angle shot gradient-echo T1-weighted sequence covering the entire brain (5.5 min) and dynamic imaging of an IV administered bolus of contrast agent with a single shot echo-planar gradient echo sequence (800/47 [TR/TE]; flip angle, 60 degrees; field of view, 24 cm; matrix, 96 × 200) covering the cerebral hemispheres with eight contiguous sections of 6-mm thickness. Each eight-section acquisition was repeated once per second, for a total imaging time of 80 s. The bolus of contrast agent consisted of a 0.2 mmol/kg dose of gadodiamide (Omniscan, Nycomed) delivered at 5 mL/s with an MR imaging-compatible power injector (Mallinckrodt, Inc.) through a large bore antecubital IV catheter.

CBF maps created from the resulting dynamic susceptibility images were generated by using the method presented by Ostergaard et al (5, 6) and publicly available software (MAKEPERF; Massachusetts General Hospital, Boston, MA). This algorithm allows deconvolution of the tissue susceptibility time curve with an AIF by using nonparametric singular value decomposition and estimates relative CBF as the amplitude of

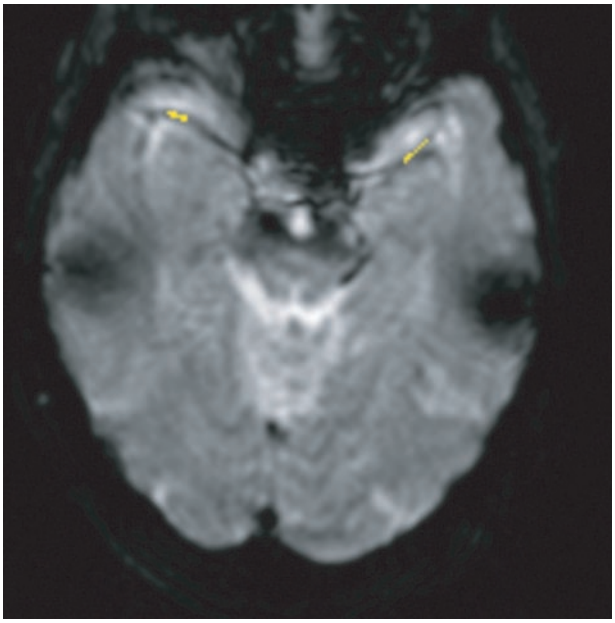

FIG 1. T2*-weighted gradient-echo single shot echo-planar transverse image (800/47; flip angle, 60 degrees), obtained at the level of the sylvian fissures in patient 7 (Table 1), who had left carotid occlusion, shows AIF selection at the M1 and M2 segments of the MCA. Pixels chosen for AIF determination are illustrated in *yellow*. Ten to 12 pixels were chosen in the MCA, both for an AIF ipsilateral to the occlusion and an AIF contralateral to the occlusion.

the resulting tissue impulse response. This is a model-independent method for determining relative CBF, in the sense that the procedure does not require any assumptions regarding the underlying tissue residue function, as does CBF measurement with [^{15}O]-H_2O PET. AIFs were manually defined by selecting 10 to 12 pixels containing the M1 or M2 segment of the MCA, located in the sylvian fissure (Fig 1). Each pixel was confirmed to contain the MCA by anatomic location within an area of flow void and by a susceptibility time curve with a steeper slope and greater amplitude than in adjacent brain parenchyma. Two CBF maps were calculated for each patient: one from an AIF ipsilateral to the occluded carotid artery and the other from an AIF contralateral to the occluded carotid artery.

PET Protocol

All PET scans were acquired with an ECAT EXACT HR PET scanner (CTI PET Systems, Knoxville, TN) in 2D mode with intersection septa extended (19). A 40-s acquisition was initiated at arrival of activity in the head after bolus injection of 1850 to 2600 MBq of [^{15}O]-H_2O, and arterial blood activity was obtained at 1-s intervals with an automated blood sampler. PET scans ($2.14 \times 2.14 \times 3.125$ mm pixels) were reconstructed with filtered back projection by using measured attenuation and scatter correction with a ramp filter. The reconstructed images were smoothed with a 3D gaussian filter to a final resolution of 10-mm full width at half-maximum in all dimensions for the region of interest analysis. Blood flow was measured by using an adaptation of the Kety autoradiographic method (20, 21). CBF values measured with [^{15}O]-H_2O PET underestimate the true CBF values at high flow rates because of the incomplete permeability of the blood-brain barrier to water. CBF values measured with PET can be corrected for the effect of finite permeability by accounting for the measured permeability-surface area product of water in the brain (22). This correction factor was applied to all CBF values measured with PET in this study by using the method presented by Herscovitch et al (22)

$$1) \qquad CBF = F/(1 - \exp(-1.50 - 20.6/F))$$

where F is the uncorrected PET blood flow obtained by using the water bolus autoradiographic method (20, 21).

To determine the degree of hemodynamic impairment in these patients and the possible impact on CBF values measured by MR imaging, PET studies of cerebral blood volume, mean transit time, and oxygen extraction fraction were also performed. Cerebral blood volume was obtained from inhaled [^{15}O]-CO experiments as previously described (23), and oxygen extraction fraction measurements were obtained by using the method presented by Mintun et al (24). Mean transit time was calculated as cerebral blood volume/CBF on a pixel-by-pixel basis. PET data were converted to atlas space, and seven spherical regions of interest were placed stereotactically within the MCA territory. Regions with previous infarction were identified based on a review of structural imaging and were excluded. Ipsilateral to contralateral hemispheric ratios of CBF, cerebral blood volume, mean transit time, and oxygen extraction fraction were calculated and compared with the range of ratios observed in 18 normal control participants (25). Those patients with ratios exceeding the normal range were considered abnormal.

CBF Region of Interest Analysis

All PET scans and MR images were co-registered and resectioned to match the original echo-planar MR images by using Automated Image Registration (26). The PET scans were co-registered to the T1-weighted 3D fast low angle shot images, which, in turn, were co-registered to the echo-planar images. CBF maps created from the MR images were smoothed with a 3D gaussian filter to match the 10-mm full width at half-maximum resolution of the PET scans.

Four 18-mm-diameter circular regions of interest were positioned in each hemisphere on each transverse section of the co-registered PET scans and MR images of each patient (Fig 2). On each transverse section, three of the four hemispheric regions contained mixed cortical/subcortical large vessel territories (anterior cerebral artery, MCA, and posterior cerebral artery), and the fourth region contained deep white matter, to define a wide range of flows. CBF was measured in the eight regions of interest from each of the five most superior sections to yield 40 corresponding flow measurements from PET and MR imaging for each patient, except two patients for whom only the four most superior sections were analyzed because of susceptibility artifacts near the skull base in the lowest section. These regions of interest were placed to avoid large vessels such as those of the circle of Willis near the skull base. MR imaging CBF calculations were made by using AIFs from the M1 or M2 segments of the MCA, both ipsilateral and contralateral to the occluded internal carotid artery. Three additional smaller regions of interest were placed in normal appearing subcortical white matter of the hemisphere contralateral to the occluded carotid artery, one in each of the three large vessel territories (Fig 2). This was performed only on the most superior section of each patient's study. For each patient, relative CBF values derived from MR imaging were converted to absolute blood flow in physically meaningful units of mL/100 mL/min under each of two separate conditions. Under the constant white matter CBF condition, this conversion was accomplished by assigning the mean relative CBF value in the three subcortical white matter regions of interest to a standard value of 22 mL/100 mL/min (6). The relative CBF values from each of the 40 large territory regions of interest were then multiplied by this individualized scaling factor to yield absolute CBF. The rationale for using normal cerebral white matter as an internal reference standard for generating absolute MR imaging CBF values is based on PET measurements showing

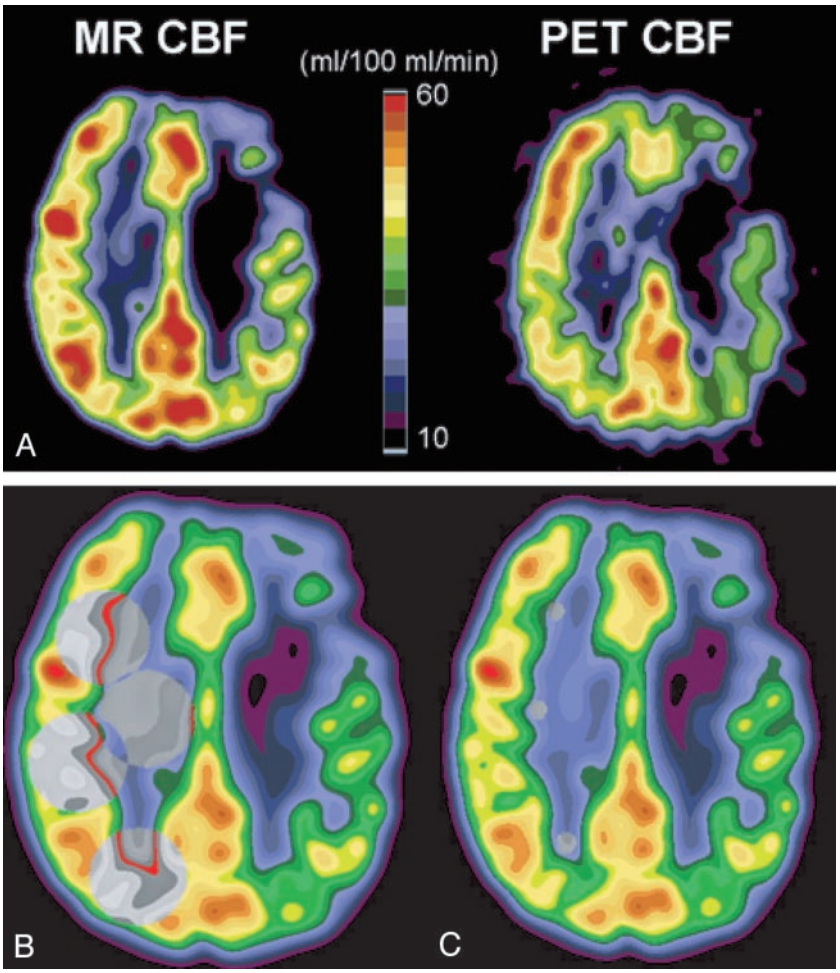

FIG 2. CBF in patient 4 (Table 1), who had occlusion of the left internal carotid artery.

A, CBF measured with dynamic susceptibility contrast-enhanced MR imaging (*MR CBF*, *left*) and CBF measured with [^{15}O]-H_2O PET (*PET CBR*, *right*). Axial view MR image and PET scan are co-registered to the same location, filtered to the same spatial resolution as the PET scan, and displayed with the same color scale. Diffusely decreased CBF in the left hemisphere, ipsilateral to the occluded carotid artery, can be identified on both the MR image and PET scan, with more severely reduced CBF focally within a chronic infarct in the left frontal lobe.

B, Large regions of interest (*gray circles*) for CBF measurement are shown on MR image obtained in the hemisphere contralateral to the carotid occlusion. Homologous regions of interest were placed in the hemisphere ipsilateral to the occlusion (see Methods).

C, Small subcortical regions of interest (*gray circles*) in normal appearing white matter of the hemisphere contralateral to the carotid occlusion are shown on MR image. These subcortical white matter regions were used to determine normal white matter CBF for the purpose of scaling relative CBF values measured by MR imaging to physically meaningful units of mL/100 mL/min (see Methods).

that in normal adult volunteers, white matter has a relatively uniform age-independent blood flow of 22 mL/100 mL/min (27). Under the PET-scaled white matter CBF condition, the ratio between the mean CBF value measured by PET and the mean relative CBF value measured by MR imaging in the three subcortical white matter regions of interest was used as a scaling factor. Relative CBF values measured by MR imaging in the 40 large hemispheric regions of interest were multiplied by this scaling factor to yield absolute CBF values measured by MR imaging in mL/100 mL/min.

Linear regression of the paired MR imaging versus PET CBF data and the linear correlation coefficient (Pearson's *r*) were calculated twice, once by using an AIF ipsilateral to the occlusion and once by using an AIF contralateral to the occlusion. Hypothesis testing was conducted by using the paired two-population two-tailed Student's *t* test. Comparison of correlation coefficients was performed after applying the Fisher z transformation to normalize their underlying distributions (28). Comparison of the slopes and y intercepts of regression lines was performed with the appropriate *t* statistic (29).

Results

Seven patients (six men and one woman; age range, 58–76 years; mean age, 67.0 years) with occlusion of the proximal internal carotid artery underwent dynamic susceptibility contrast-enhanced MR imaging and PET (Table 1). Five patients had left-sided occlusion, and two had right-sided occlusion. Four patients had a history of cortical infarction ipsilateral to the occluded carotid artery, whereas three were asymptomatic with no history of stroke or transient ischemic attack.

Figure 2 provides illustrative examples of an MR image and an anatomically co-registered PET scan of a patient with left carotid occlusion who had a chronic left frontal lobe infarct. Reduced CBF throughout the hemisphere ipsilateral to the occluded carotid artery, and more severely decreased CBF focally within the left frontal infarct, are shown on both MR images and PET scans.

For all seven patients, a statistically significant correlation was shown between CBF values measured by MR imaging and CBF values measured by PET (Table 2). The linear correlation coefficients ranged from 0.50 to 0.88, all of which were statistically significant at $P < .001$. No significant difference was observed in the PET/MR imaging correlation coefficient for any of the seven patients between CBF values measured by MR imaging and obtained with an AIF ipsilateral versus those measured by MR imaging and obtained contralateral to the occluded carotid artery ($P > .05$). The choice of AIF did not significantly affect the slope or y intercept of the observed MR imaging versus PET CBF regression lines for six of the seven patients ($P > .05$). For these six patients, no appreciable difference was observed between the AIFs ob-

TABLE 1: Participant clinical data and position emission tomography hemodynamic parameters

Participant	Age/Sex/ Handedness	Side of Occlusion	Clinical History	PET			
				CBF	CBV	MTT	OEF
1	67/M/R	L	Asymptomatic	0.85	0.89	1.05	1.02
2	65/F/R	L	Asymptomatic	0.84	0.95	1.13	1.03
3	58/M/R	L	Left parietal infarct	0.89	**1.30**	**1.46**	**1.09**
4	67/M/L	L	Left posterior frontal infarct	0.87	1.10	**1.26**	0.93
5	71/M/R	R	Asymptomatic	0.96	1.13	**1.17**	0.98
6	76/M/R	R	Right posterior parietal infarct	0.98	1.17	**1.19**	1.04
7	65/M/R	L	Left frontoparietal infarct	0.80	1.09	**1.37**	1.06

All positron emission tomography hemodynamic parameters are ipsilateral-to-contralateral ratios of mean hemispheric values. Cerebral blood volume, mean transit time, and oxygen extraction fraction ratios that exceed the range observed in 18 normal control participants are shown in bold text. The upper limits for normal hemispheric ratios for cerebral blood volume, mean transit time, and oxygen extraction were 1.21, 1.14, and 1.08, respectively. Hemodynamic impairment is clearly shown for participant 3. Participants 4 through 7 may have some degree of autoregulatory vasodilation, with elevated mean transit times.

Note.—PET indicates positron emission tomography; CBF, cerebral blood flow; CBV, cerebral blood volume; MTT, mean transit time; OEF, oxygen extraction fraction; M, male; F, female; R, right; L, left.

TABLE 2: Results of linear regression of cerebral blood flow values measured by MR imaging versus cerebral blood flow values measured by positron emission tomography

Participant	Ipsilateral AIF			Contralateral AIF		
	r	Slope	y-int.*	*r*	Slope	y-int.*
1	0.65	0.48	9.30	0.66	0.47	9.11
2	0.75	0.70	2.63	0.72	0.67	4.42
3	0.50	0.42	20.8	0.62	0.55	15.9
4	0.88	1.04	5.20	0.85	0.88	9.10
5	0.88	0.94	0.38	0.88	0.97	0.27
6	0.80	1.05	−9.44	0.82	1.17	−14.7
7	0.79	1.65	−5.74	0.81	2.14	−17.7
Pooled†	0.60	0.55 ± 0.05	16.6 ± 1.99	0.54	0.54 ± 0.05	17.6 ± 2.26

For each participant and for the pooled data, the linear correlations between cerebral blood flow values measured by MR imaging and cerebral blood flow values measured by by positron emission tomography, both for ipsilateral and contralateral arterial input functions, are statistically significant ($P < .001$).

* y-intercepts of regression lines are expressed in mL/100 mL/min.

† Mean linear regression parameters of pooled data from all seven participants (Fig 5A) and standard errors of the mean for slopes and y-intercepts of regression lines.

Note.—AIF indicates arterial input function; y-int., y intercepts of the regression lines. The slopes represent cerebral blood flow values measured by MR imaging versus cerebral blood flow values measured by positron emission tomography and therefore are dimensionless.

tained from the MCAs ipsilateral and contralateral to the occlusion (Fig 3). For patient 7, a statistically significant difference ($P < .05$) was shown in the slope of the regression line obtained under the two AIF conditions (Fig 4A). This patient was also the only one to exhibit a delayed, broadened AIF in the MCA ipsilateral to the carotid occlusion (Fig 4B).

Figure 3 shows good quantitative agreement between CBF values measured by MR imaging and those measured by PET in regions of interest from both cerebral hemispheres in a 71-year-old man with asymptomatic right carotid occlusion. However, for other patients, the quantitative CBF values measured by MR imaging and those measured by PET diverged more widely. The pooled data from all seven participants (Fig 5A) showed considerable scatter around the line of identity, with CBF values measured by MR imaging underestimating CBF values measured by PET in some cases and overestimating CBF values measured by PET in other cases. This is also reflected by the wide variation among patients in the PET CBF regression lines versus the MR imaging CBF regression lines (Table 2), many of which depart considerably from the ideal slope of 1 and the ideal y intercept of 0. The regression line through the pooled MR imaging versus PET CBF data (Fig 5A) shows that across all patients, MR imaging tended to overestimate CBF at low flow rates and to underestimate CBF at high flow rates. This results in a slope significantly <1 and a y intercept significantly >0 for the pooled MR imaging versus PET regression line, both for the ipsilateral AIF and the contralateral AIF (Table 2). The choice of AIF made no statistically significant difference in the correlation coefficient, slope, or y intercept of the pooled MR imaging versus PET regression line ($P > .05$).

One source of the discrepancies between quantitative CBF values measured by PET and those mea-

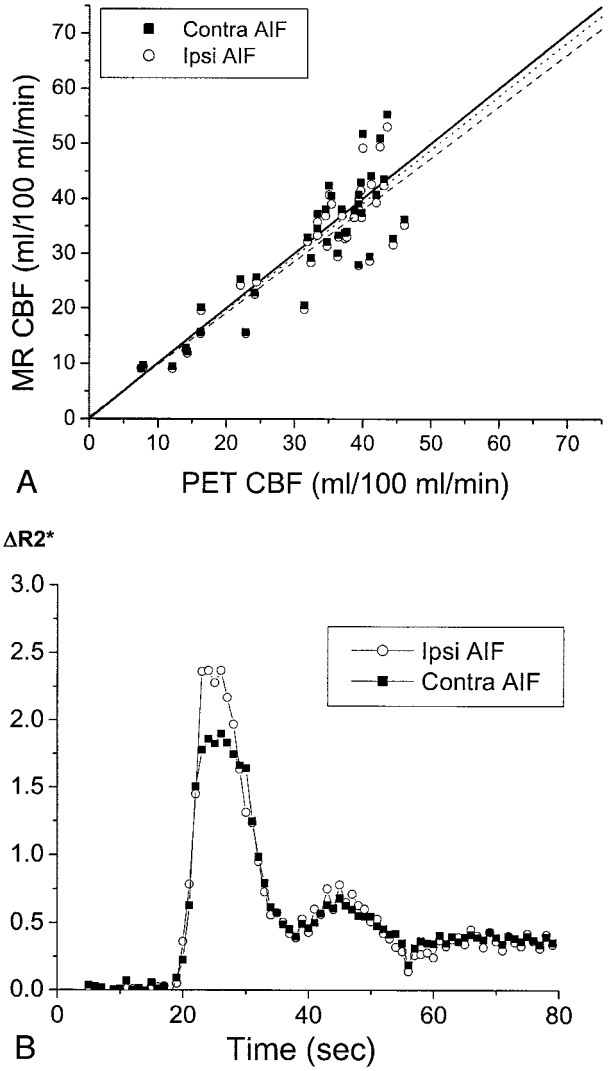

FIG 3. CBF in patient 5, a 71-year-old man who had chronic right carotid occlusion.

A, Graph compares CBF values measured by MR imaging (*MR CBF*) with those measured by PET (*PET CBF*). CBF values measured by PET have been corrected for the finite permeability of water through the blood-brain barrier (see Methods). CBF values measured by MR imaging were calculated with AIFs from the proximal MCA, both ipsilateral to the occluded carotid artery (*Ipsi AIF*, *open circles*) and contralateral to the occluded carotid artery (*Contra AIF*, *closed squares*). The line of identity, with a slope of 1 and a y intercept of 0, is depicted by a *solid line*. The slopes of the regression line for the data from the ipsilateral AIF (*dashed line*) and for the data from the contralateral AIF (*dotted line*) are both close to 1 (Table 2). No statistically significant difference was observed in the slopes or y intercepts of the two regression lines ($P > .05$). The linear relationship between CBF values measured by MR imaging and those measured by PET is statistically significant for both the ipsilateral AIF ($r = 0.88$, $P < .0001$) and the contralateral AIF ($r = 0.88$, $P < .0001$). CBF values measured by PET in the subcortical white matter regions used in scaling the CBF values measured by MR imaging was 21.1 mL/100 mL/min, which is close to the assumed value of 22 mL/100 mL/min (see Methods).

B, Plots of the relaxivity ΔR2* versus time for the AIF in the M1 or M2 segment of the MCA ipsilateral to the carotid occlusion (*open circles*), and that contralateral to the occlusion (*closed squares*), show that they are almost identical. ΔR2* was determined as the negative log of susceptibility after baseline normalization. Because susceptibility is a relative measurement and not an absolute quantity, ΔR2* is expressed in arbitrary units. The amplitude of the observed change in ΔR2* is not quantitatively comparable between the ipsilateral and contralateral sides because of differences in factors such as vessel orientation and the extent of partial volume averaging of the blood vessel with surrounding tissue and/or CSF within the selected AIF pixels.

sured by MR imaging was the variability of blood flow within the reference white matter regions used to scale the MR imaging measurements to absolute units of mL/100 mL/min. The CBF values measured by PET in these white matter regions ranged from 21 to 45 mL/100 mL/min among patients. This resulted in large scaling errors in the CBF values measured by MR imaging for those patients in whom the actual white matter blood flow, measured with PET, departed considerably from the assumed value of 22 mL/100 mL/min. Use of the white matter flow rates measured with PET for each patient to scale the CBF values measured by MR imaging for that patient to absolute units resulted in an improvement in the correlation between CBF values measured by PET and those measured by MR imaging (Fig 5B). For the ipsilateral AIF, the R^2 value, expressing the percentage of the variance in CBF values measured by MR imaging across all patients explained by CBF values measured by PET, increased from 36% to 72%. Similarly, for the contralateral AIF, the R^2 value improved from 29% to 71%. With this correction for flow variability in white matter, the resulting regression lines through the pooled data for both AIFs had slopes significantly >1 ($P < .0001$) and y intercepts significantly <0 ($P < .05$).

Discussion

We have shown that blood flow measurements obtained with dynamic susceptibility contrast-enhanced MR imaging are significantly correlated with quantitative CBF values derived from [^{15}O]-H_2O PET in all seven of our patients with chronic unilateral carotid occlusion. Although a significant linear relationship existed between CBF values measured by MR imaging and those measured by PET for every patient and in the pooled data from all patients, the slope and y intercept of the regression lines varied widely among patients. Thus, although dynamic susceptibility contrast-enhanced MR imaging may provide a good qualitative index of CBF, it does not yield accurate quantitative values of absolute CBF in individual patients with cerebrovascular disease. These findings are consistent with those reported by Lin et al (10) who also noted significant linear correlations between CBF values measured by MR imaging and those measured by PET for each of five patients with unilateral carotid occlusion but large differences in the slope of the relationship.

The relatively poor accuracy of absolute CBF values measured by MR imaging relates to the general issue of how to convert a susceptibility signal intensity with no intrinsic measurement units into an absolute flow rate with physically meaningful units of mL/100

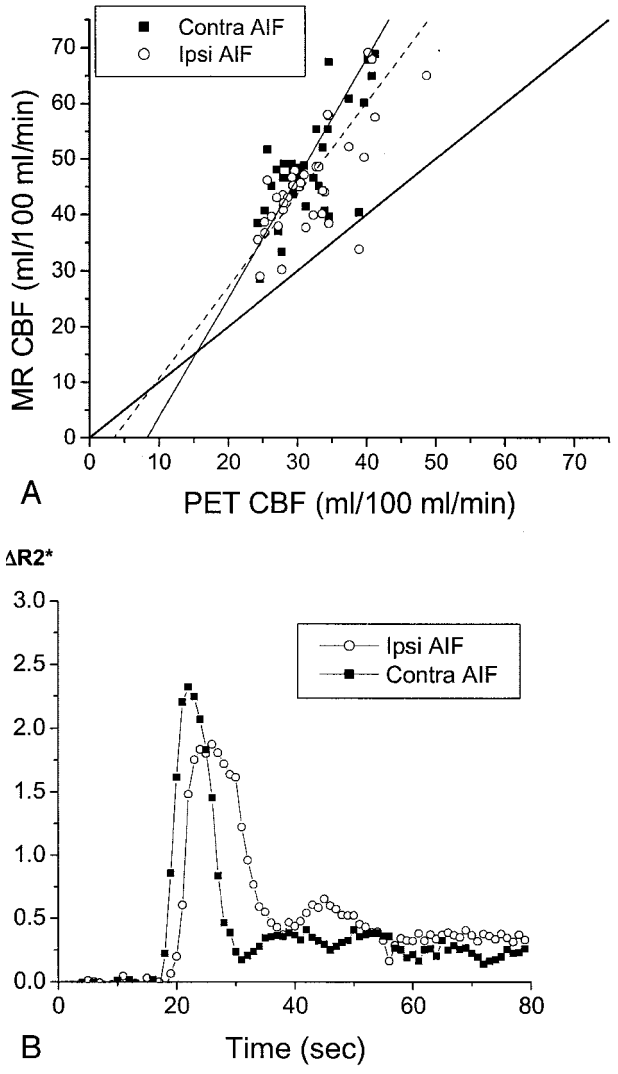

FIG 4. Delay and dispersal of the AIF ipsilateral to the occluded carotid artery affects calculated CBF values measured by MR imaging (*MR CBF*). Conventions used are as described in the legend to Figure 3.

A, In a 65-year-old man with symptomatic left carotid occlusion (patient 7), CBF values measured by MR imaging systematically overestimated CBF values measured by PET (*PET CBF*). The linear regression between CBF values measured by MR imaging and those measured by PET has a slope of 1.65 for the ipsilateral AIF (*Ipsi AIF*, $r = 0.79$, $P < .0001$) and 2.14 for the contralateral AIF (*Contra AIF*, $r = 0.81$, $P < .0001$). This difference in slopes is statistically significant ($P < .05$). CBF value measured by PET in the subcortical white matter regions used in scaling the CBF values measured by MR imaging was 21.9 mL/100 mL/min, which is very close to the assumed value of 22 mL/100 mL/min.

B, AIFs in patient 7 show a delay in the peak of the ipsilateral AIF (*open circles*) and a broader peak of the ipsilateral AIF, compared with the contralateral AIF (*closed squares*).

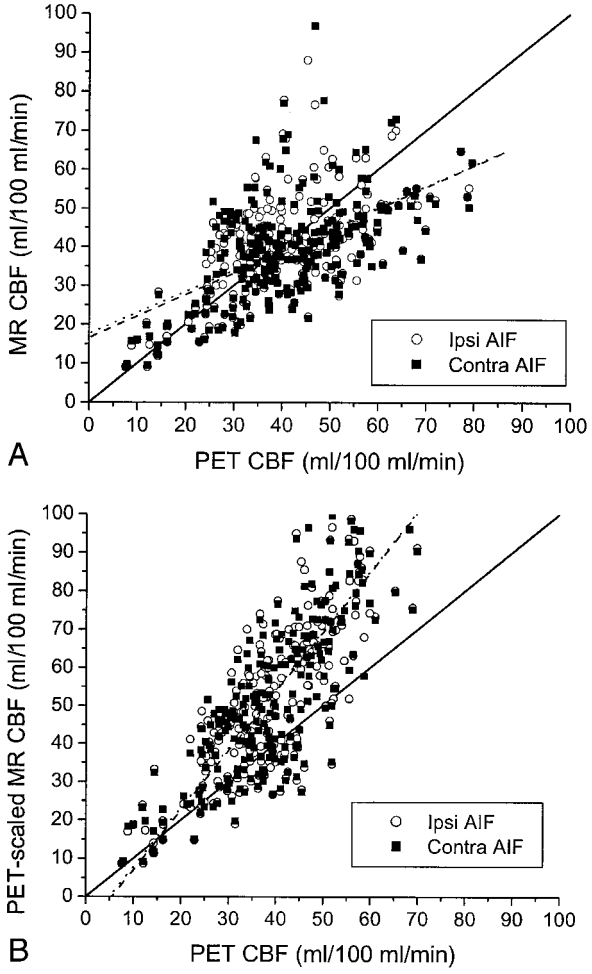

FIG 5. CBF in all seven patients.

A, Pooled data from all seven patients shows a statistically significant correlation between CBF values measured by MR imaging (*MR CBF*) and CBF values measured by PET (*PET CBF*), when CBF values measured by MR imaging are calculated with an AIF ipsilateral to the carotid occlusion (*Ipsi AIF*, *open circles*) ($r = 0.60$, $P < .0001$) and with an AIF contralateral to the occlusion (*Contra AIF*, *closed squares*) ($r = 0.54$, $P < .0001$). No significant differences were observed between the correlation coefficients, slopes, or y intercepts of the regression lines for the ipsilateral AIF (*dashed line*) and the contralateral AIF (*dotted line*). Both regression lines have slopes significantly <1 ($P < .001$) and y intercepts significantly >0 ($P < .001$). Relative MR CBF values were scaled to absolute units by assuming a normal white matter flow rate of 22 mL/100 mL/min (see Methods).

B, Use of white matter flow rates measured with PET for each patient to scale relative CBF values measured with MR imaging for each patient to absolute units improves the correlation between CBF values measured by MR imaging and those measured by PET, both for the ipsilateral AIF (*open circles*) ($r = 0.85$, $P < .0001$) and the contralateral AIF (*closed squares*) ($r = 0.84$, $P < .0001$). Again, no significant difference was observed between the correlation coefficients, slopes, or y intercepts of the regression lines for the ipsilateral AIF (*dashed line*) and the contralateral AIF (*dotted line*). However, both regression lines for PET-scaled CBF values measured by MR imaging versus CBF values measured by PET have slopes significantly >1 ($P < .001$) and y intercepts significantly <0 ($P < .05$).

mL/min. One approach to this problem, first used by Ostergaard et al (6), is to use a constant internal white matter reference flow rate to scale relative CBF values measured by MR imaging to absolute values. This solution is based on the observation that measurements of white matter CBF obtained by PET of normal volunteers have a uniform, age-independent value of 22 mL/100 mL/min (27). Although white matter CBF may be relatively constant in normal adult volunteers, our measurements obtained by PET showed wide variability (21–45 mL/100 mL/min) in patients with chronic carotid occlusion, in the hemi-

sphere contralateral to the occlusion, leading to systematic underestimation of absolute CBF values measured by MR imaging for some patients (Fig 5A). Correcting this white matter flow variability by using measurements of white matter CBF obtained by PET to scale the relative CBF values measured by MR imaging to absolute units improves the correlation between CBF values measured by MR imaging and those measured by PET (Fig 5B).

Another source of error in CBF values measured by MR imaging is delay and dispersal of the bolus of contrast agent (5, 6, 13). Delay and dispersal of the bolus may arise from factors related to IV administration, such as injection rate and caliber of the venous cannula, or it may be caused by host factors such as cardiac output. Because all our patients were power injected at a standardized rate, with no evident problems at the injection site, variation in host factors is the more likely explanation for differences across patients in the measured AIFs. Also, underestimation of the AIF causes overestimation of the calculated CBF values measured by MR imaging (9). Underestimation of the AIF may occur because of inadequate temporal resolution in sampling the AIF or partial volume averaging of the artery with adjacent brain parenchyma or CSF. AIF underestimation seemed to be worst in patient 7, in whom the slopes of the MR imaging versus PET CBF regression lines were the greatest (Fig 4A, Table 2). After correction for white matter flow variability, the pooled data across all patients showed that CBF values measured by MR imaging systematically overestimated those measured by PET (Fig 5B). This indicates that underestimation of AIF may have occurred to varying extents for all seven patients. Because the caliber of the proximal MCA is only approximately 2 mm, whereas the section thickness of the MR imaging acquisition is 6 mm, partial volume averaging of the AIF should be expected for every patient.

Previous studies have used additional postprocessing steps to derive quantitative estimates of absolute CBF values measured by dynamic susceptibility contrast-enhanced MR imaging by empirically correcting for underestimation of the AIF due to partial volume averaging. One approach has been to normalize the area under the AIF curve to the injected dose of contrast agent and to then apply an empiric correction factor, common across all patients, to the calculated CBF values measured by MR imaging to convert them to absolute flow rates in physically meaningful units of mL/100 mL/min (7, 8). This method has yielded good quantitative correspondence between MR imaging and PET measurements of absolute CBF in normal human volunteers (8) but has not been validated in patients with cerebrovascular disease. Another approach is to measure the contrast agent concentration time curve in the superior sagittal sinus, to determine the venous output function, and to compute a correction factor that is individual to each patient and that can convert MR imaging blood flow measurements to absolute CBF values in terms of mL/100 mL/min (10). The resulting changes in scale were largely successful in standardizing the slopes of the MR imaging versus PET blood flow regression lines to values close to unity in a group of five patients with unilateral carotid occlusion (10). However, variation remained in the y intercepts of the regression lines, reducing the accuracy of the quantitative CBF estimates measured by MR imaging, especially at low flow rates. Also, all these methods for deriving absolute CBF values measured by MR imaging assume linearity between contrast agent concentration and the measured T2*-weighted signal intensity decrease. Experimental measurements have found some nonlinearity in this relationship (30), and linearity is explicitly violated in cases in which there is truncation of the measured signal intensity at 0. The techniques for generating absolute CBF measurements from dynamic susceptibility contrast-enhanced MR imaging are not widely used clinically, and we did not use them, considering that our purpose was to evaluate the accuracy of CBF values estimated based on MR imaging by using the methodology that is currently in the most widespread clinical use.

We examined the effect on CBF values measured by MR imaging of AIFs chosen ipsilateral to the carotid occlusion versus those contralateral to the occlusion. For six of the seven patients, no appreciable difference was observed between the two AIFs and no statistically significant difference ($P < .05$) was observed between CBF values measured by MR imaging based on the two AIFs (Fig 3). The seventh patient did exhibit delay and dispersal of the bolus of contrast agent in the MCA ipsilateral to the carotid occlusion, and this did significantly influence the CBF values measured by MR imaging ($P < .05$) (Fig 4). The delay in the ipsilateral AIF may be the most important factor, because singular value decomposition is known to be sensitive to contrast agent arrival delays (5, 6, 13, 15).

Patient seven also had a moderate degree of hemodynamic compromise in the cerebral hemisphere ipsilateral to the occlusion, as evidenced by a history of ipsilateral cortical infarction and by a markedly elevated mean transit time ratio (Table 1). However, the other six patients, for whom there were no differences in CBF values measured by MR imaging attributable to AIF selection, exhibited degrees of hemodynamic compromise varying from none in two asymptomatic patients (patients 1 and 2) to severe in a symptomatic patient (patient 3) with both elevated oxygen extraction fraction and elevated cerebral blood volume (16, 18). We observed no systematic differences in the performance of dynamic susceptibility contrast-enhanced MR imaging for the measurement of CBF based on these differences in hemodynamic status. It is important to note that we measured cerebral blood volume, mean transit time, and oxygen extraction fraction in mixed cortical and subcortical regions within the MCA territory. This was done for two reasons. First, the regions of interest for CBF values measured by MR imaging AIF sampling were placed in the MCA as well. Second, the identical regional analysis was used in previous stud-

ies correlating hemodynamic impairment with stroke risk (18, 25).

In this study, we used PET as the gold standard method of comparison for MR imaging measurements of CBF. However, for several reasons, including the two enumerated below, PET is not an ideal technique for absolute CBF quantitation. First, one assumption of the water-bolus PET autoradiographic method for CBF measurement (20) is that the time-activity curve of radiotracer in the radial artery is the same as in the intracranial arteries. This may not hold true in patients with occlusive disease and collateral channels of flow. The impact of this on the accuracy of CBF values measured by PET is not known but is likely less critical than for MR imaging or CT methods of measuring CBF using the first pass of nondiffusible plasma tracers. The PET method relies on integration of radioactivity counts during a 40-s time period by using a freely diffusible radiotracer, compared with the first pass study of a plasma tracer. Second, the PET and MR imaging measurements were not simultaneous. Some change in CBF after transfer from the MR imaging unit to the PET scanner, or vice versa, might be expected.

In summary, for six of seven patients with chronic unilateral carotid occlusion, including some symptomatic patients with PET evidence of ipsilateral hemodynamic compromise, the AIFs did not differ between hemispheres. In only one symptomatic patient with evidence of hemodynamic compromise was a delayed, broadened AIF found ipsilateral to the occlusion, and this was the only patient who showed significant differences in CBF values measured by MR imaging due to AIF selection ($P < .05$). These findings in association with chronic carotid occlusive disease differ from what has been described in association with acute ischemia. In cases of acute ischemia, delay and dispersal of the bolus of contrast agent is commonly encountered distal to the occluded artery, and, in these instances, AIF selection has been shown to affect quantitative hemodynamic parameters obtained from dynamic susceptibility contrast-enhanced MR imaging (15) and the spatial extent of the hemodynamic abnormality on parametric maps (14).

Conclusion

Dynamic susceptibility contrast-enhanced MR imaging, by allowing deconvolution of the tissue susceptibility time curve with the AIF, can provide a good qualitative index of CBF for patients with chronic carotid occlusion. However, direct comparison with the results of [^{15}O]-H_2O PET shows that without additional postprocessing steps, these CBF values do not constitute a reliable quantitative measure of absolute CBF in individual patients with chronic cerebrovascular disease. The two dominant sources of error in absolute CBF values measured by MR imaging were 1) variability in blood flow in white matter regions used to scale relative CBF values measured by MR imaging to absolute units, causing 2) underestimation of true flow rates, and underestimation of the AIF, leading to overestimation of true flow rates. The choice of AIF, relative to the side of carotid occlusion, had no significant influence on the CBF values measured by MR imaging for six of seven patients ($P > .05$), because the AIFs did not differ between the two sides. However, one patient with symptomatic carotid occlusion did exhibit delay and dispersal of the AIF ipsilateral to the occlusion, which did significantly affect the calculated CBF values measured by MR imaging. These findings differ from those presented in published studies of dynamic susceptibility contrast-enhanced MR imaging in the setting of acute ischemia. Further studies with correlation to clinical end points are needed to determine the usefulness of relative CBF values measured by MR imaging for patients with pathologic cerebral hemodynamics.

Acknowledgments

We thank Joshua S. Shimony, MD, PhD, for many helpful discussions regarding perfusion imaging and for access to beta versions of a custom perfusion analysis software.

References

1. Sorensen AG, Copen WA, Ostergaard L, et al. **Hyperacute stroke: simultaneous measurement of relative cerebral blood volume, relative cerebral blood flow, and mean tissue transit time.** *Radiology* 1999;210:519–527
2. Knopp EA, Cha S, Johnson G, et al. **Glial neoplasms: dynamic contrast-enhanced T2*-weighted MR imaging.** *Radiology* 1999;211:791–798
3. Ernst TM, Chang L, Witt MD, et al. **Cerebral toxoplasmosis and lymphoma in AIDS: perfusion MR imaging experience in 13 patients.** *Radiology* 1998;208:663–669
4. Rempp KA, Brix G, Wenz F, Becker CR, Guckel F, Lorenz WJ. **Quantification of regional cerebral blood flow and volume with dynamic susceptibility contrast-enhanced MR imaging.** *Radiology* 1994;193:637–641
5. Ostergaard L, Weisskoff RM, Chesler DA, Gyldensted C, Rosen BR. **High resolution measurement of cerebral blood flow using intravascular tracer bolus passages: part I. mathematical approach and statistical analysis.** *Magn Reson Med* 1996;36:715–725
6. Ostergaard L, Sorensen AG, Kwong KK, Weisskoff RM, Gyldensted C, Rosen BR. **High resolution measurement of cerebral blood flow using intravascular tracer bolus passages: part II. experimental comparison and preliminary results.** *Magn Reson Med* 1996;36:726–736
7. Ostergaard L, Smith DF, Vestergaard-Poulsen P, et al. **Absolute cerebral blood flow and blood volume measured by magnetic resonance imaging bolus tracking: comparison with positron emission tomography values.** *J Cereb Blood Flow Metab* 1998;18:425–432
8. Ostergaard L, Johannsen P, Host-Poulsen P, et al. **Cerebral blood flow measurements by magnetic resonance imaging bolus tracking: comparison with [^{15}O]-H_2O positron emission tomography in humans.** *J Cereb Blood Flow Metab* 1998;18:935–940
9. Smith AM, Grandin CB, Duprez T, Mataigne F, Cosnard G. **Whole brain quantitative CBF, CBV, and MTT measurements using MRI bolus tracking: implementation and application to data acquired from hyperacute stroke patients** *J Magn Reson Imaging* 2000;12:400–410
10. Lin W, Celik A, Derdeyn C, et al. **Quantitative measurements of cerebral blood flow in patients with unilateral carotid artery occlusion: a PET and MR study.** *J Magn Reson Imaging* 2001;14:659–667
11. Sakoh M, Rohl L, Gyldensted C, Gjedde A, Ostergaard L. **Cerebral blood flow and blood volume measured by magnetic resonance imaging bolus tracking after acute stroke in pigs: comparison with [^{15}O]-H_2O positron emission tomography.** *Stroke* 2000;31:1958–1964

12. Calamante F, Gadian DG, Connelly A. **Quantification of perfusion using bolus tracking magnetic resonance imaging in stroke: assumptions, limitations, and potential implications for clinical use.** *Stroke* 2002;33:1146–1151
13. Calamante F, Gadian DG, Connelly A. **Delay and dispersion effects in dynamic susceptibility contrast MRI: simulations using singular value decomposition.** *Magn Reson Med* 2000;44:466–473
14. Neumann-Haefelin T, Wittsack HJ, Fink GR, et al. **Diffusion- and perfusion-weighted MRI: influence of severe carotid artery stenosis on the DWI/PWI mismatch in acute stroke.** *Stroke* 2000;31:1311–1317
15. Yamada K, Wu O, Gonzalez RG, et al. **Magnetic resonance perfusion-weighted imaging of acute cerebral infarction: effect of the calculation methods and underlying vasculopathy.** *Stroke* 2002;33:87–94
16. Powers WJ, Press GA, Grubb RL Jr, Gado M, Raichle ME. **The effect of hemodynamically significant carotid artery disease on the hemodynamic status of the cerebral circulation.** *Ann Intern Med* 1987;106:27–35
17. Derdeyn CP, Grubb RL Jr, Powers WJ. **Cerebral hemodynamic impairment: methods of measurement and association with stroke risk.** *Neurology* 1999;53:251–259
18. Derdeyn CP, Videen TO, Yundt KD, et al. **Variability of cerebral blood volume and oxygen extraction: stages of cerebral haemodynamic impairment revisited.** *Brain* 2002;125:595–607
19. Weinhard H, Dahlbom M, Eriksson L, et al. **The ECAT EXACT HR: performance of a new high resolution positron scanner.** *J Comput Assist Tomogr* 1994;18:110–118
20. Herscovitch P, Markham J, Raichle ME. **Brain blood flow measured with intravenous H2(15)O: I. theory and error analysis.** *J Nucl Med* 1983;24:782–789
21. Videen TO, Perlmutter JS, Herscovitch P, Raichle ME. **Brain blood volume, blood flow, and oxygen utilization measured with O-15 radiotracers and positron emission tomography: revised metabolic computations.** *J Cereb Blood Flow Metab* 1987;7:513–516
22. Herscovitch P, Raichle ME, Kilbourn MR, Welch MJ. **Positron emission tomographic measurement of cerebral blood flow and permeability: surface area product of water using [15O] water and [11C] butanol.** *J Cereb Blood Flow Metab* 1987;7:527–542
23. Martin WR, Powers WJ, Raichle ME. **Cerebral blood volume measured with inhaled C15O and positron emission tomography.** *J Cereb Blood Flow Metab* 1987;7:421–426
24. Mintun MA, Raichle ME, Martin WR, Herscovitch P. **Brain oxygen utilization measured with O-15 radiotracers and positron emission tomography.** *J Nucl Med* 1984;25:177–187
25. Grubb RL Jr, Derdeyn CP, Fritsch SM, et al. **Importance of hemodynamic factors in the prognosis of symptomatic carotid occlusion.** *JAMA* 1998;280:1055–1060
26. Woods RL, Mazziotta JC, Cherry SR. **MRI-PET registration with automated algorithm.** *J Comput Assist Tomogr* 1993;17:536–546
27. Leenders KL, Perani D, Lammertsma A, et al. **Cerebral blood flow, blood volume and oxygen utilization: normal values and effect of age.** *Brain* 1990;113:27–47
28. Zar JH. *Biostatistical Analysis.* 4th ed. Upper Saddle River: Prentice Hall; 199:381–388
29. Zar JH. *Biostatistical Analysis.* 4th ed. Upper Saddle River: Prentice Hall; 1999:360–368
30. Weisskoff RM, Zuo CS, Boxerman JL, Rosen BR. **Microscopic susceptibility variation and transverse relaxation: theory and experiment.** *Magn Reson Med* 1994;31:601–610